The diffuse transition between the Zagros continental collision and the Makran oceanic subduction (Iran): microearthquake seismicity and crustal structure

Farzam Yamini-Fard, Denis Hatzfeld, A. M. Farahbod, Anne Paul, M. Mokhtari

Geophys. J. Int. (2007) **170,** 182–194 doi: 10.1111/j.1365-246X.2006.03232.x

The diffuse transition between the Zagros continental collision and the Makran oceanic subduction (Iran): microearthquake seismicity and crustal structure

F. Yamini-Fard,[1,2] D. Hatzfeld,[1] A. M. Farahbod,[2] A. Paul[1] and M. Mokhtari[2]

[1]*Laboratoire de Géophysique Interne et Tectonophysique, UJF-CNRS,* BP 53, 38041 *Grenoble Cedex* 9, *France. E-mail: denis.hatzfeld@ujf-grenoble.fr*
[2]*International Institute of Earthquake Engineering and Seismology,* PO Box 19395/3913, *Tehran, Iran*

Accepted 2006 September 20. Received 2006 September 20; in original form 2006 March 24

SUMMARY

The nature of the transition between the Zagros intra-continental collision and the Makran oceanic subduction is a matter of debate: either a major fault cutting the whole lithosphere or a more progressive transition associated with a shallow gently dipping fault restricted to the crust. Microearthquake seismicity located around the transition between the transition zone is restricted to the west of the Jaz-Murian depression and the Jiroft fault. No shallow microearthquakes seem to be related to the NNW–SSE trending Zendan–Minab–Palami active fault system. Most of the shallow seismicity is related either to the Zagros mountain belt, located in the west, or to the NS trending Sabzevaran–Jiroft fault system, located in the north. The depth of microearthquakes increases northeastwards to an unusually deep value (for the Zagros) of 40 km. Two dominant types of focal mechanisms are observed in this region: low-angle thrust faulting, mostly restricted to the lower crust, and strike-slip at shallow depths, both consistent with NS shortening. The 3-D inversion of *P* traveltimes suggests a high-velocity body dipping northeastwards to a depth of 25 km. This high-velocity body, probably related to the lower crust, is associated with the deepest earthquakes showing reverse faulting. We propose that the transition between the Zagros collision and the Makran subduction is not a sharp lithospheric-scale transform fault associated with the Zendan–Minab–Palami fault system. Instead it is a progressive transition located in the lower crust. The oblique collision results in partial partitioning between strike-slip and shortening components within the shallow brittle crust because of the weakness of the pre-existing Zendan–Minab–Palami faults.

Key words: collision, Iran, Makran, seismicity, subduction, tomography, Zagros.

INTRODUCTION

The transition between a continental collision and an active oceanic subduction zone is a classical example of a discontinuity in kinematic boundary conditions. Most of these collision–subduction transition zones are associated with a sharp single fault that behaves as a transform fault, where seismicity is high, such as in Western Greece (Baker *et al.* 1997), in Taiwan (Kao *et al.* 1998), or in New Zealand (Anderson *et al.* 1993). In this paper, we investigate the transition zone between the Zagros collision and the Makran subduction whose surface expression is related to the active Zendan–Minab–Palami (hereafter called ZMP) fault system (Fig. 1).

Iran lies between the lithospheric plates of Arabia and Eurasia which converge at approximately 25 mm yr^{-1} (Vernant *et al.* 2004). West of ∼57°E, the related shortening is accommodated by folding and thrust faulting in the Zagros mountain belt in the southwest and in the Alborz and Kopeh Dagh mountains in the north, and by slip on several major strike-slip faults (mostly trending NS) in Iran. East of ∼57°E, convergence results in the Makran subduction zone associated with the Makran accretionary prism located south of the Jaz-Murian depression (Fig. 1).

The Zagros, a NW–SE trending fold-and-thrust mountain belt, is located on the Mesozoic passive margin of the Arabian plate. It runs for ∼1200 km between the North Anatolian fault in the NW and the Makran subduction zone in the SE. The Zagros mountain belt is bounded to the NE by the Main Zagros Reverse Fault located on the former active boundary between Arabia and Iran (e.g. Berberian 1995). A thick sedimentary sequence ranging continuously from the Cambrian to Quaternary overlies the Precambrian basement (e.g. Stöcklin 1974). The Zagros Folded Belt resulted from the continental collision that followed the completion of oceanic subduction. The beginning of the continental collision is still debated and estimates range between the late Cretaceous (e.g. Stöcklin 1974) to the late Miocene (e.g. Stoneley 1981). The present day shortening of the Zagros is estimated by GPS measurements to be ∼10 mm yr^{-1} (Tatar *et al.* 2002; Vernant *et al.* 2004; Hessami *et al.* 2006) and the total

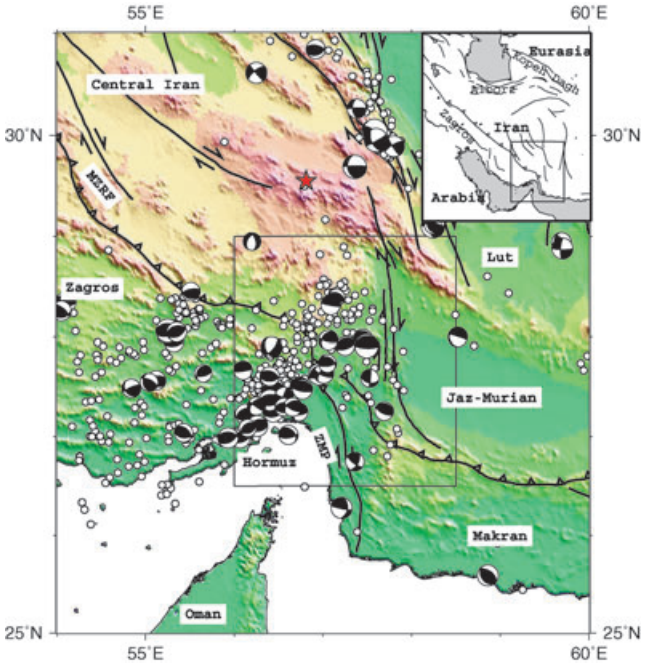

Figure 1. Location of the Zendan–Minab–Palami fault system at the transition between the Zagros collision, on the west and the Makran subduction on the east. Seismicity is the relocated catalogue form Engdahl *et al.* (1998). The red star is the 107 km deep earthquake. Focal mechanisms are CMT solutions (http://www.seismology.harvard.edu/CMTsearch.html). We report the main faults from Talebian & Jackson (2004), Regard *et al.* (2004) and Molinaro *et al.* (2005). The box is the Zendan–Minab–Palami area (Fig. 3). The inset shows the geographical setting.

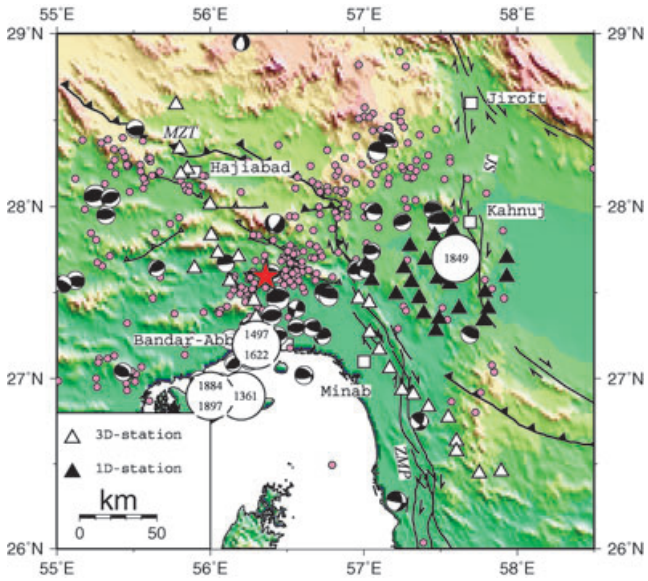

Figure 2. Instrumental seismicity (Engdahl *et al.* 1998) as pink dots, historical seismicity for Iran (Ambraseys & Melville 1982) as large circles with numbers, and major faults (Regard *et al.* 2004; Molinaro *et al.* 2005) of the Zagros-Makran transition zone. Black triangles are 1-D seismographs used to locate the seismicity. White triangles are the 3-D seismological stations used to study the velocity structure across the ZMP fault system. The red star shows the location of the 1977 March 21, Khurgu earthquake (Ms = 7.0).

amount of the Zagros shortening is thought to be between ∼50 km (Blanc *et al.* 2003; Molinaro *et al.* 2005) and ∼85 km (McQuarrie 2004). This shortening has been accommodated by reverse faulting in the basement (Jackson 1980; Berberian 1995) partially or completely decoupled from the active folding of the shallow sediments (Blanc *et al.* 2003; Walpersdorf *et al.* 2006). Reverse faulting, located in the basement beneath the sedimentary cover, accounts for many of the larger earthquakes and most activity in accurate microearthquake surveys, which are generally restricted to depths less than 20 km (Talebian & Jackson 2004; Tatar *et al.* 2004).

The Makran subduction, between Arabia and Iran or India, is related to the active subduction of the Indian oceanic crust beneath Iran and Eurasia at a rate of about 40 mm yr^{-1} since the Early Cretaceous (Farhoudi & Karig 1977). The Makran subduction is associated with one of the world's largest accretionary wedges, ∼350 km wide, several km thick and active since the Oligocene. This wedge is composed of siliclastic sediments deposited in the Oman Gulf (e.g. Harms *et al.* 1984), and is growing seawards at a rate of about 1 cm yr^{-1} (White 1982). The seismic zone associated with the Makran subduction zone dips at a very low angle and is associated with low level intermediate-depth seismicity, mostly with dip-slip mechanisms (Jacob & Quittemeyer 1979; Byrne *et al.* 1992; Maggi *et al.* 2000).

To investigate the geometry and the kinematics of the transition between the collision and the subduction, we deployed a local temporary network around Minab (Fig. 2) for 50 days. We complemented this network with a line of stations across the ZMP fault system to study the crustal and upper-mantle structures.

TECTONIC SETTING

The transition between the Zagros collision and the Makran subduction is located near the Hormuz Strait at the Zendan-Minab-Palami fault system, also called the Oman line (e.g. Gansser 1964; Shearman 1977; Kadinsky-Cade & Barazangi 1982). At the surface, the ZMP fault system connects the Main Zagros Reverse Fault, north of the Zagros mountain belt, to the thrust faults in the south of the Makran accretionary prism, but it is not connected clearly to the Makran Trench located off the coast. This excludes the ZMP from being a classic Transform Fault. Ophiolites are seen both along the MZRF in the Zagros and in Oman (i.e. McCall & Kidd 1982). In both places, they are of Mesozoic age and were obducted onto the Arabian margin during the late Cretaceous (e.g. Stöcklin 1968; McCall & Kidd 1982). Since the Eocene time, the history of the Zagros and Oman diverge because of the closure of the Tethys in the Zagros and the onset of the collision, whereas the subduction is still active beneath Makran.

The NW–SE ZMP fault system carries southwestward flysh of Oligo-Miocene age as well as ophiolitic nappes (also called coloured mélanges) of late Cretaceous age onto the Zagros units of Paleocene age. The coloured mélanges are interpreted to be the remnant of sediments scraped off during the pre-collision subduction episode (McCall & Kidd 1982).

Locally, the ZMP fault system affects the Zagros folds which rotate parallel to the ZMP system, leading Sattarzadeh *et al.* (2000) to suggest that it is a transpressive fault system. On the other hand, Regard *et al.* (2004) differentiate between a spatial separation, during the upper Miocene-Pliocene of pure reverse faulting and an en-échelon folding, followed by a more homogeneous Plio-Quaternary transpressional regime. This would explain the slight rotation with time of the principal compressive strain orientation from ENE–WSW to NE–SW along the ZMP fault system. Molinaro *et al.*

(2004) associate the change in the folding across the ZMP fault zone to a difference in the depth of the deformation that involves an efficient décollement at a depth of 8 km in the west but a more frictional slip at 6 km depth in the east. The intense seismicity associated with NS shortening in the Zagros is clearly bounded in the east by the ZMP fault zone, further east of which the deformation is aseismic (e.g. Quittemeyer 1979; Kadinsky-Cade & Barazangi 1982; Talebian & Jackson 2004). Northeast of the ZMP, the NS striking right-lateral strike-slip Jiroft and Sabzevaran faults, only a few tens of km long, participate in the NS striking strike-slip system that transfers part of the differential motion between Central Iran and the Lut block to the Nayband fault system located further North (Walker & Jackson 2002).

GPS measurements, both with the global Iranian network (Vernant *et al.* 2004) and with a local network installed across the fault system (Bayer *et al.* 2006) confirm a right lateral motion of $\sim$10 mm yr^{-1} on the ZMP fault system. Assuming rigid blocks separated by faults locked at 15 km, Bayer *et al.* (2006) infer a total of $\sim$15 mm yr^{-1} of strike-slip motion associated with $\sim$6 mm yr^{-1} of shortening between the Zagros mountains and the Makran accretionnary prism. The present day strike-slip motion across the Jiroft Sabzevaran fault is only $\sim$3 mm yr^{-1} (Bayer *et al.* 2006), but was as much as 6 mm yr^{-1} during the Quaternary (Regard *et al.* 2005).

The historical seismicity is significant around the Straight of Hormuz (Quittemeyer 1979; Ambraseys & Melville 1982), but it is not well documented (Fig. 2) because of the relatively sparse population living in this area. Most earthquakes are located west of Bandar-Abbas, in the Zagros mountain belt. A single event (1849) occurred near Khanuj (Fig. 2) which is not well documented. At sea, several strong events of magnitude greater than *Ms* $\sim$ 7 are related to rupture along the plate boundary in the Makran subduction (Byrne *et al.* 1992). One event in 1483, located in the west of the subduction zone is uncertain and could possibly be related either to the Zagros or to the Zagros-Makran transition (Byrne *et al.* 1992). No shallow seismicity is unambiguously associated with the ZMP fault zone itself.

The instrumental seismicity confirms that the lack of historical shallow seismicity related to the ZMP fault zone and to the Makran subduction is probably not an artifact due to the remoteness of the area (Quittemeyer 1979; Quittemeyer & Jacob 1979; Byrne *et al.* 1992). It also confirms that instrumental earthquakes are located west of the ZMP fault zone (Berberian & Tchalenko 1976). Their mechanisms are mostly reverse on an $\sim$EW trending fault plane, as is the case for the Kurghu earthquake of 1977 (Berberian *et al.* 1977; Kadinsky-Cade & Barazangi 1982). Sparse seismicity is related to the Makran subduction, mostly in the easternmost side, and focal mechanisms show reverse-slip mechanisms. This lack of earthquakes in the western Makran may indicate a different tectonic behaviour from that in the eastern Makran: either that subduction is aseismic, or that it is presently locked (Byrne *et al.* 1992). The easternmost Zagros is the only place, within the Zagros, where focal depths increase northeastwards, with at least two events at 28 km depth, deeper than is usual in the Zagros (Maggi *et al.* 2000; Talebian & Jackson 2004). This deepening is probably related to the underthrusting of Arabia beneath Central Iran in this area (Kadinsky-Cade & Barazangi 1982; Snyder & Barazangi 1986; Talebian & Jackson 2004). One earthquake (1970, November 9; 29.55°N, 56.81°E) located at a depth of 100 km is probably related to the Makran subduction (Maggi *et al.* 2000).

The only microearthquake study conducted in this area (Niazi 1980) deployed 5 land-based seismometers and 3 Ocean Bottom Seismographs for 2 weeks in 1977. Most of the recorded activity was related to the 1977 Kurghu earthquake and no activity was detected in association with the ZMP fault zone.

DATA

From 1999 November 17 to 2000 January 6, we maintained a network of 24 short-period one-component seismological stations in the region of Minab to study the local seismicity and the crustal structure (black triangles in Fig. 2). Each station was equipped with a 12-bit digitizer, recording in a trigger mode at a sampling frequency of 100 Hz, and connected to a 2-Hz vertical seismometer and to a GPS time receiver. This network was complemented by a profile of 25 seismological stations installed to study the crustal and upper-mantle velocity structure on both sides of the ZMP fault system (white triangles in Fig. 2). This second set of stations was equipped with 24-bit digitizers recording in a continuous mode at 125 Hz and connected to 3-D sensors, either broad-band seismometers CMG40, middle-band Le3D seismometers, or short-period L22 seismometers. Time was calibrated every hour with a GPS time receiver. During the nearly 50-day period, we recorded 496 local events, with a minimum of 3 *P*-arrival and 2 *S*-arrival times.

Little is known about the crustal velocity structure in the ZMP region, and we chose to estimate it from our local data. Firstly, we calculated a *Vp*/*Vs* ratio of 1.759 $\pm$ 0.004 using 3634 Tsj-Tsi vs Tpj-Tpi (*S* and *P* in all stations) arrival times. Secondly, we selected a subset of 172 events recorded with a minimum of five *P* and two *S* arrival times, an rms value less than 0.2 s, uncertainties both in epicentre (ERH) and in depth (ERZ) less than 2 km, and an azimuthal gap less than 180°. With this selected subset of events, we performed a 1-D inversion using the VELEST program (Kissling 1988) to get the most appropriate velocity structure. Because the resulting structure is strongly dependent on the starting velocity model, we explored 50 initial models randomly distributed (with differences as large as 0.5 km s^{-1} in each layer) around our initial starting model (Paul *et al.* 2001). We kept only the resulting models for which the 1-D inversion converges correctly (i.e. the rms decreases significantly to values less than 0.06 s). We proceeded in 2 steps, first we look for the largest discontinuities in the velocity structure, and then for the most appropriate velocities in each of the main layers. We started with a velocity structure composed of a stack of layers 2 km thick, of uniform velocity 6.0 km s^{-1}. This multilayered model allowed us to determine the depth of the largest velocity discontinuities. The result of this inversion suggests that no more than three layers are necessary to describe the velocity structure. We therefore performed a second 1-D inversion with a reduced number of three layers that were again randomly perturbed to obtain the final model (Table 1).

Focal mechanisms are computed for earthquakes with a minimum of eight first-motion polarities (Table 2). We take into consideration the quality of the azimuthal coverage on the focal sphere and the possibility of alternative solutions in order to distribute the solutions into three categories depending on their reliability. We put the mechanisms for which four quadrants are sampled and the two planes are constrained within 20° in category A. In category B, only three quadrants are sampled and the two planes are well constrained.

Table 1. 1-D velocity structure.

Vp (km s^{-1})	depth (km)
5.70	0
6.50	8
8.20	40

Table 2. Parameters of the focal mechanisms.

Number	Date	Time	lat	lon	Depth	Mag	Az1	pl1	de1	Az2	pl2	de2	Azp	dep	Azt	det	Q
7	991118	13:25	27.73	57.42	19	2.1	135	80	89	320	10	94	225	35	43	5	B
8	991118	16:39	27.64	57.41	20	2.3	95	55	25	350	69	142	45	9	307	40	A
10	991118	17:02	27.64	57.41	20	1.4	95	55	25	350	69	142	45	9	307	40	D
15	991119	18:13	27.69	57.78	21	2.9	261	85	18	170	71	174	34	9	127	16	A
23	991121	15:55	27.60	57.28	17	2.2	130	40	90	310	50	90	40	5	220	85	B
28	991122	00:29	27.64	57.41	19	1.2	95	55	25	350	69	142	45	9	307	40	D
33	991122	06:48	27.76	57.57	17	2.2	100	40	37	340	67	123	45	15	292	54	C
46	991123	22:18	27.77	57.46	17	2.3	187	44	60	46	52	115	118	4	15	69	A
48	991123	23:10	27.76	57.45	17	2.3	183	44	61	40	52	114	112	4	10	70	A
49	991123	23:17	27.76	57.45	17	2.0	199	35	54	61	61	112	134	14	11	65	A
65	991125	12:25	27.57	57.32	22	1.7	257	81	6	166	83	170	211	1	121	10	C
73	991126	21:36	27.77	57.65	19	1.1	100	38	−93	285	52	−86	212	82	12	7	C
77	991127	04:52	27.64	57.44	20	2.0	120	33	77	315	57	98	39	12	248	75	A
99	991130	06:32	27.64	57.40	20	2.0	90	60	9	355	81	149	46	14	308	27	B
111	991201	03:18	27.16	57.82	15	3.3	250	70	14	155	76	159	203	4	111	24	B
113	991201	12:45	27.61	57.79	21	3.0	162	15	−90	342	75	−90	252	60	72	30	B
116	991201	14:36	27.61	57.72	13	1.7	112	85	38	18	51	173	238	22	342	30	A
123	991202	15:45	27.54	57.46	15	0.9	110	80	90	290	10	90	200	35	20	55	D
145	991206	20:02	27.59	57.57	21	2.9	278	35	76	115	56	99	198	10	55	76	A
152	991207	02:51	27.81	57.61	25	1.5	283	80	−50	25	40	−164	229	41	343	24	D
153	991207	05:00	27.83	56.45	15	1.2	90	70	90	270	20	90	180	25	65	D	
156	991207	09:02	27.65	57.38	17	1.9	77	80	−21	171	68	−169	32	22	125	7	A
179	991210	21:41	27.79	57.63	22	1.2	115	67	90	295	23	90	205	22	25	68	D
183	991211	09:11	27.45	56.86	38	3.5	250	75	−7	342	82	−164	206	15	115	5	A
190	991211	22:49	27.67	57.27	37	1.3	250	66	−29	353	63	−152	210	37	302	1	B
194	991212	16:55	27.77	57.39	21	1.0	110	80	90	290	10	90	200	35	20	55	D
198	991212	17:10	27.78	57.39	20	1.0	304	20	80	135	70	93	222	25	50	64	B
203	991212	17:13	27.78	57.41	21	2.9	304	20	80	135	70	93	222	25	50	64	A
204	991212	17:20	27.77	57.40	20	1.7	304	19	80	135	71	93	222	26	50	63	B
205	991212	17:22	27.77	57.40	20	1.8	304	15	79	135	75	92	222	30	48	59	B
206	991212	17:29	27.78	57.41	21	1.8	304	18	94	120	72	88	211	27	27	62	A
207	991212	18:51	27.78	57.40	21	1.5	300	15	90	120	75	90	210	30	30	60	B
209	991212	19:41	27.78	57.39	21	1.1	304	20	79	135	70	93	222	25	51	64	D
218	991213	16:16	27.78	57.41	19	1.3	304	25	94	120	65	88	211	20	26	69	D
219	991213	18:04	27.82	57.46	23	2.6	50	40	−6	145	85	−129	20	36	266	29	B
220	991213	19:54	27.67	57.38	14	0.7	120	85	90	290	5	80	209	40	31	50	D
221	991213	20:08	27.83	57.62	17	2.6	105	28	−81	275	62	−94	174	72	8	17	B
242	991216	18:38	27.45	57.48	18	1.2	125	60	90	305	30	90	215	15	35	75	B
273	991221	01:52	27.43	57.53	8	1.9	290	80	−26	25	63	−168	244	25	340	11	A
274	991221	04:25	27.44	57.53	7	3.4	285	80	−11	17	78	−169	240	15	331	0	A
275	991221	18:10	27.47	57.85	15	2.1	250	65	11	155	79	154	204	9	110	25	C
296	991222	19:09	27.82	57.62	2	2.5	280	57	−90	100	33	−90	190	78	10	12	A
298	991222	19:33	27.81	57.61	21	1	95	30	−98	285	60	−85	208	74	11	15	D
304	991222	21:39	27.81	57.62	18	1.6	275	65	−90	95	25	−90	185	70	5	20	B
306	991223	00:14	27.67	57.77	24	1.0	170	75	161	265	72	15	217	2	127	23	D
307	991223	03:22	27.43	57.52	11	2.7	277	62	−22	18	70	−150	239	34	146	5	A
308	991223	09:10	27.44	57.53	10	3.1	285	65	−11	20	79	−154	245	25	150	9	A
310	991223	20:20	27.70	57.47	39	1.3	325	45	−90	145	45	−90	149	90	55	C	
317	991224	19:41	27.62	57.47	15	1.2	110	80	90	290	10	90	200	35	20	55	B
320	991225	17:34	27.58	57.47	11	1.0	100	70	−90	280	20	−90	10	65	190	25	C
321	991225	17:41	27.89	57.69	32	3.8	130	73	137	235	49	22	187	14	84	41	C
326	991225	20:18	27.56	57.85	6	1.5	60	20	−90	240	70	−90	150	65	330	25	D
331	991226	19:10	27.81	57.62	23	2.6	78	82	89	259	8	91	168	37	347	53	B
332	991227	01:30	27.71	57.34	6	1.0	140	72	86	330	18	99	232	26	45	62	D
343	991228	00:37	27.44	57.44	13	1.4	120	80	90	300	9	90	210	35	30	54	B
381	991231	13:44	27.43	57.53	9	2.0	10	75	161	105	72	15	57	2	327	23	A
387	991231	15:03	27.79	57.51	19	1.4	90	80	−90	270	10	−90	55	180	35	C	
391	991231	16:24	27.79	57.50	19	1.1	90	80	−90	270	10	−90	55	180	35	C	
397	991231	20:48	27.63	57.47	15	0.9	105	80	90	285	10	90	195	35	15	55	D
403	991231	22:56	27.82	57.62	24	1.4	280	10	99	90	80	88	181	35	357	54	B
405	991231	22:58	27.81	57.61	23	1.3	280	10	99	90	80	88	181	35	357	54	B
407	991231	23:11	27.81	57.61	26	1.1	280	10	99	90	80	88	181	35	357	54	B
409	991231	23:30	27.82	57.62	24	1.3	280	10	99	90	80	88	181	35	357	54	
410	991231	23:32	27.81	57.61	25	1.0	270	8	99	80	82	88	171	37	348	52	B

Table 2 – (*Continued.*)

Number	Date	Time	lat	lon	Depth	Mag	Az1	pl1	de1	Az2	pl2	de2	Azp	dep	Azt	det	Q
414	991231	23:40	27.81	57.61	25	1.1	255	8	90	75	82	90	165	37	345	53	B
415	991231	23:40	27.82	57.61	24	1.1	255	8	90	75	82	90	165	37	345	53	D
420	991231	23:46	27.82	57.61	26	1.1	255	8	90	75	82	90	165	37	345	53	B
421	991231	23:52	27.81	57.61	25	1.7	255	8	85	80	82	90	169	37	350	53	B
422	991231	23:53	27.82	57.61	26	1.3	90	83	90	270	7	90	180	38	360	52	D
423	991231	23:59	27.82	57.62	26	1.9	285	5	112	82	85	88	173	40	349	49	B
424	000101	00:02	27.81	57.61	24	2.0	270	5	98	82	85	89	172	40	351	49	B
429	000101	00:32	27.81	57.61	23	0.9	95	78	89	280	12	94	185	33	3	57	D
439	000101	02:45	27.82	57.61	27	1.1	95	83	89	280	7	95	185	38	4	52	D
443	000101	04:16	27.90	57.68	30	2.6	130	80	134	230	45	14	187	21	79	38	C
446	000101	12:54	27.71	57.77	24	1.5	183	78	−170	91	80	−12	46	15	137	1	B
447	000101	16:37	27.79	57.50	17	1.2	55	40	90	235	50	90	325	5	145	85	D
453	000102	00:37	27.51	57.56	22	1.0	110	80	90	290	10	90	200	35	20	55	D
458	000102	10:48	27.79	57.66	17	2.0	263	62	−26	6	67	−149	226	37	133	3	B
463	000102	15:13	27.78	57.66	17	1.1	265	77	−20	0	70	−166	221	23	314	4	B
468	000103	00:04	27.578	57.31	23	1.1	110	45	20	5	75	133	64	18	316	42	D
473	000104	01:19	27.49	57.28	6	1.2	102	80	28	7	61	168	232	12	328	27	B
484	000104	22:01	27.47	57.47	7	1.1	272	74	10	179	79	163	226	3	134	18	A
486	000105	02:42	27.77	57.81	18	1.8	95	75	90	275	15	90	185	30	5	60	C

Lat, Lon are the coordinates of the earthquake. Mag is the magnitude. Az, pl, de are Azimuth, dip and slip of fault plane 1 and 2. Azp, dep, Azt, det are azimuth and dip of *P*- and *T*-axis, respectively. A, B and C are a factor quality.

In category C, only two quadrants are sampled, and alternative solutions are possible.

MICROSEISMICITY DISTRIBUTION

First, we relocated a total of 496 events recorded by a minimum of 3-P and 2-S arrival times, but with no other selection criteria using Hypo71 (Lee & Stewart 1975) in the appropriate velocity structure (Fig. 3). This gives us an image (although blurred by uncertain locations that can reach 4 km) of the seismic activity over the whole area with no selection due to the network coverage and azimuthal gap. The epicentral distribution of seismicity is scattered between the Zagros folded belt in the west and the Jaz Murian depression in the east. It is clearly bounded to the east by the NS trending Jiroft fault and by the Jaz-Murian depression which is totally free of microearthquakes, even those at subcrustal depths (and therefore possibly related to the subduction). This sharp cut-off of seismic activity is well constrained by the location capabilities of the seismological network, which provides ample coverage of the ZMP-Jiroft-Sabzevaran fault system. No earthquake is associated with the ZMP fault system itself. This is not an effect of the seismological network distribution because we recorded earthquakes west of the network, in the Zagros fold belt, at larger hypocentral distances. Actually, the largest magnitudes were observed for earthquakes located in the Zagros fold belt, as on the USGS seismicity map, some of which may be continuing aftershock activity from the large magnitude ($Ms = 7.0$) Kurgu event of 1977 (Berberian 1995).

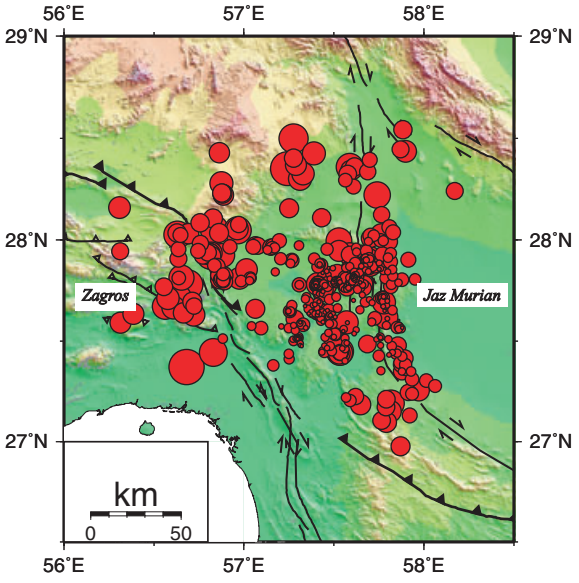

Figure 3. Epicentral distribution of all the 496 events recorded in Zagros-Makran transition zone from 1999 November 17 to 2000 January 6. The size of the symbol is proportional to the magnitude of the event (ranging between 0.2 and 3.6). The seismicity is spread between the ZMP and the JS fault zones but is clearly bounded in the east by the Jaz Murian depression.

To refine our interpretation, we selected the 309 events that fulfil the following selection criteria: number of *P* arrivals > 6, rms < 0.2 s, ERH and ERZ < 2 km, and azimuthal gap < 270° (Fig. 4). This selection of seismicity is restricted to earthquakes within, or close to, the network, in the Jiroft-Sabzevaran fault area, because of the gap criterion. Therefore, it does not allow us to extend our conclusions to the ZMP fault system or the subduction zone. This selection of epicentres is still scattered between the ZMP and the JS fault systems and does not make it possible to identify single faults associated with the seismic activity. However, we observe a clear northeastward deepening of the hypocenters. The deepest events are located at 40 km depth which is rather unusual in the Zagros (Fig. 4). Elsewhere in the Zagros, earthquakes depths are shallower than 15 km in Central Zagros, around Qir (Tatar *et al.* 2004), or in Northern Zagros, around Borujen (Yamini-Fard *et al.* 2006; Talebian & Jackson 2004), located further north.

In order to eliminate scatter due to local heterogeneities in the velocity structure and to refine our interpretation, we relocated all earthquakes (with no selection criteria) using the double difference method HypoDD (Waldhauser & Ellsworth 2000). If the hypocentral distance between events is small compared to the distance to the

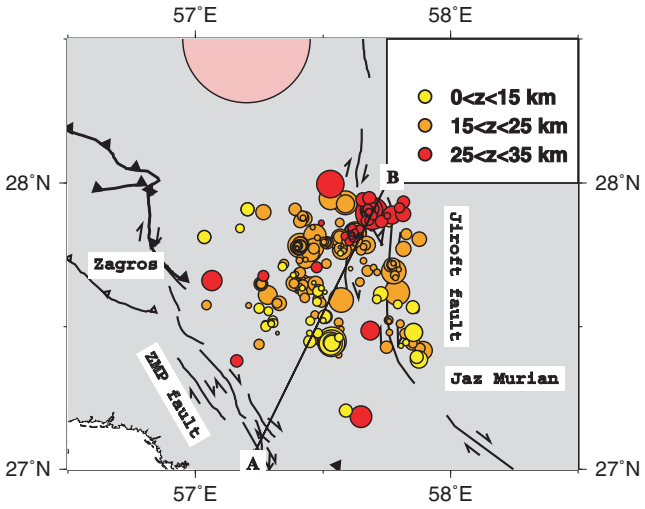

Figure 4. Epicentral distribution of 309 selected (rms < 0.2 s, ERH and ERZ < 2 km, gap < 270°) events in transition zone. Symbol size as for the previous figure. No clear fault is identified but there is a clear deepening of the hypocenters northwards. The large red circle is the location of the teleseismically located deeper events (Talebian & Jackson 2004).

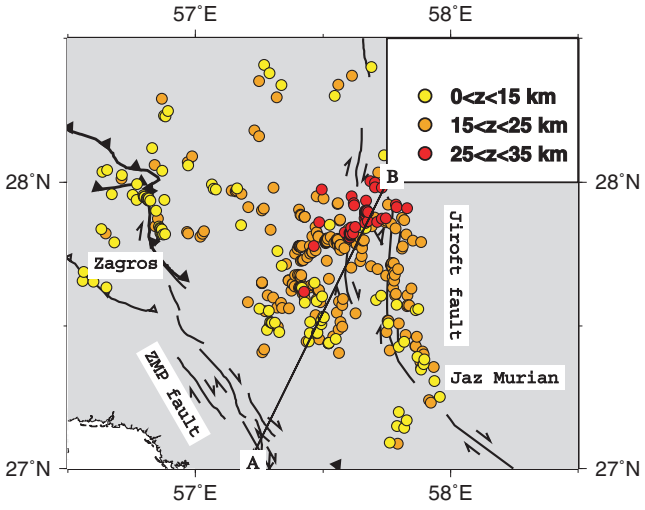

Figure 5. Epicentral distribution of the 449 earthquakes located by the relative location procedure HypoDD (Waldhauser & Ellsworth 2000) in order to avoid any systematic bias due to local heterogeneities in the velocity structure. There is no scaling of the size related to the magnitude of the earthquakes.

stations, the effects of velocity anomalies on the ray path are minimized by HypoDD because it locates events relative to each other within clusters. This method is particularly useful to map clusters of earthquakes related to possible active faults. We choose to have linked pairs of events when we have a minimum of five traveltimes to stations and distances between events smaller than 10 km. The corresponding seismicity map (Fig. 5) that includes 449 events confirms that seismicity is scattered between the ZMP and the JS faults. It also confirms the northeastward deepening of the hypocenters down to 35 km, but it does not allow to identify individual active faults.

This NE deepening is better seen on a cross-section trending NE, perpendicular to the ZMP fault system and to the trend of the deepest hypocenters (Fig. 6). In this cross-section, we report both

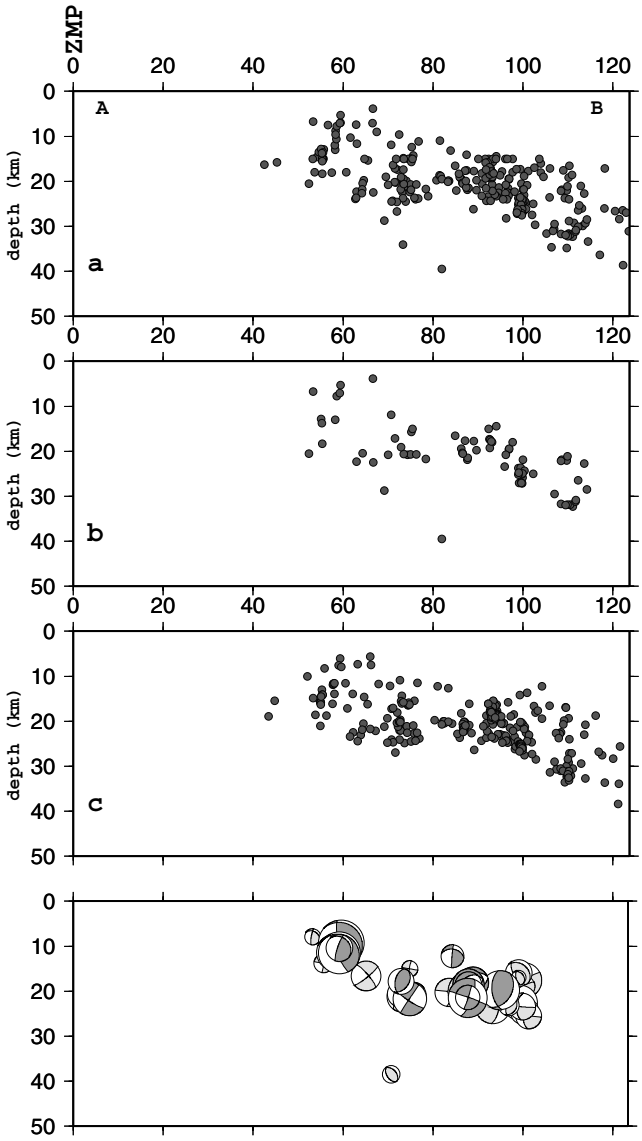

Figure 6. Cross-sections trending NNE-SSW, parallel to the convergence direction between Arabia and Jaz-Murian (Bayer *et al.* 2006). (a) from the total set of events (Fig. 3) located with Hypo71; (b) from the 309 selected events (Fig. 4) with N > 6, rms < 0.2 s, ERH and ERZ < 2 km; (c) from the 449 double difference relocated events (Fig. 5) with HypoDD (Waldhauser & Ellsworth 2000), (d) back hemisphere of the focal mechanisms projected onto the section (see Figs 4 and 5). The black mechanisms are quality A and the grey mechanisms are quality B (see the text). The width of the section is 20 km. The ZMP fault is reported on the top.

the complete data set, the selected data set, and the HypoDD data set. All show similar features and the deepening of the seismicity is confirmed, down to a depth of 40 km. This dipping seismicity is located ∼50 km SE of the NE deepening seismicity described by Talebian and Jackson (2004), and could be related to the same overthrusting mechanism (see Fig. 4).

FOCAL MECHANISMS

We computed 16 mechanisms of quality A, 31 of quality B, and 12 of quality C (see above). The mechanisms are not uniformly distributed in the area, but they are distributed into several clusters of similar

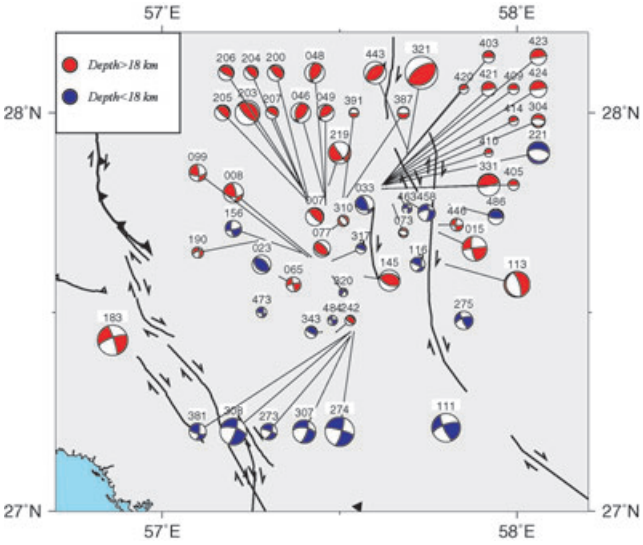

Figure 7. Map of the focal mechanisms of quality A–C. Blue mechanisms are shallower than 18 km and red are deeper than 18 km.

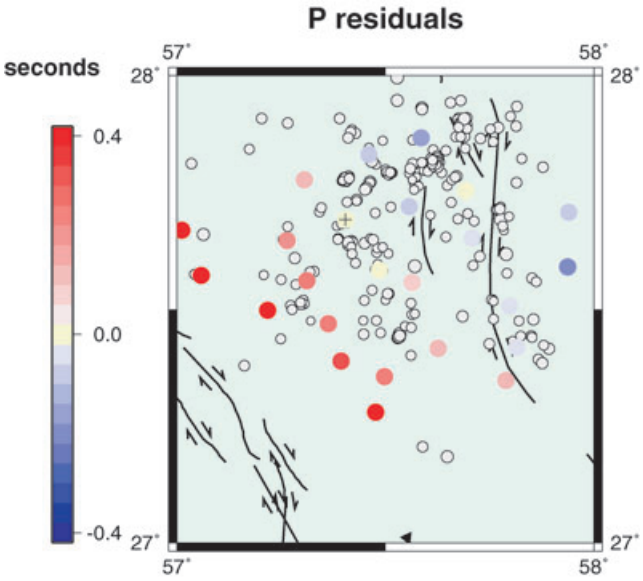

Figure 8. *P*-residuals at the seismological stations after 1-D inversion.

pattern (Fig. 7). We observe both reverse and strike-slip mechanisms. Most of the strike-slip mechanisms are located to the south and are dextral if we choose the NS striking nodal plane (parallel to the Jiroft and Sabzevaran faults) as the active fault plane. The reverse mechanisms are spread between EW striking planes (for earthquakes located in the east in one cluster) or NW–SE striking planes (for earthquakes located in the west). A few mechanisms located in the middle have a NE-SW (#321, 443) or a NW–SE (#007, 077, 242) striking plane. The type of mechanisms is not randomly distributed with depth: most of the reverse mechanisms are deeper than 18 km and located in the north, whereas most of the strike-slip mechanisms are shallower than 18 km. Earthquakes of such small magnitude cannot be related unambiguously to individual large faults, but at least they provide an image of the strain accommodation in the crust. One possible interpretation is therefore that shallow earthquakes reflect the deformation on NS striking right-lateral faults, such as the Jiroft and Sabzevaran strike-slip faults, and that the deepest events are related to a thrust décollement beneath them. Another interpretation, which does not exclude the former, is that the upper crust fails on pre-existing NS striking faults, striking obliquely to the shortening direction, whereas the lower crust involves reverse faulting of a different orientation. This will be discussed later on.

3-D VELOCITY STRUCTURE INVERSION

Residuals after the 1-D inversion show a clear regional pattern (Fig. 8). Residuals are positive (late arrival times) for stations located in the SW of the network and negative (early arrival times) for stations located in the NE, with a maximum difference that reaches ∼0.8 s. This consistent pattern of residuals is probably due to lateral heterogeneities in the velocity structure, which could be related to the active tectonics in this area. To further investigate the velocity

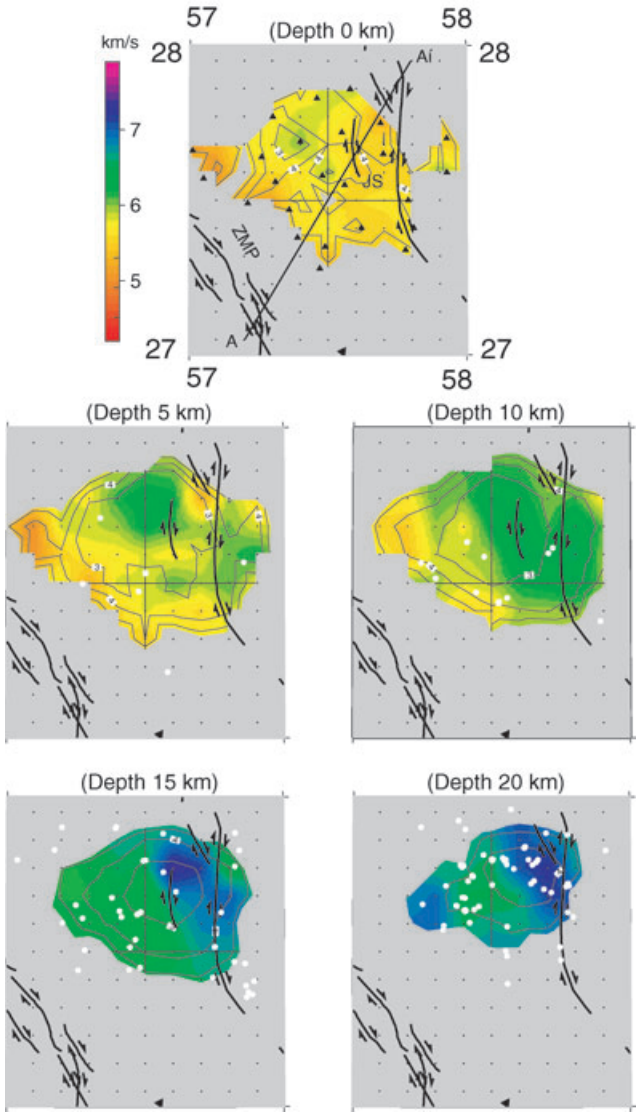

Figure 9. Maps of the velocity anomaly computed from inversion of the traveltime of local events in the seismological network. The results are for slices at different depth. On the slice 0 km, we report the seismological stations, the velocity anomaly scale, and the location of the cross-section (AA′). In each slice we report the hypocenters located in the slice. The results are reported only for a spread function (see the text) less than 5.

structure we inverted the arrival times simultaneously for velocity and for hypocenter parameters using the SIMULPS12 program (Thurber 1993; Evans *et al.* 1994). We followed Paul *et al.* (2001) for the details in the procedure and the choice of the different parameters of the inversion. As for the initial velocity structure, we used the 1-D inversion model and the 228 hypocenters that fulfil the following criteria: GAP $\leq 270^{\circ}$, rms ≤ 0.2 s and a minimum of five *P* and three *S* recorded phases. In total we used 3568 arrival times (2185 *P* and 1383 *S*). We divided the crust into blocks with a horizontal dimension of 10 km, comparable to the average distance between stations, sufficient to investigate large-scale heterogeneities in the crust. We computed the velocity for layers at 0, 5, 10, 15 and 20 km. The shallowest layer mostly accommodates the station corrections. We chose a damping factor of 100, after testing different relations between the data variance and the model variance that did not produce significant change in the resulting model. We selected a large damping factor of 10 000 for the *Vp*/*Vs* ratio to eliminate instabilities due to possible errors in reading the *S* arrival times. Finally, we stopped the inversion after seven iterations because no noticeable reduction in the variance (∼54 per cent) was observed for more iterations.

Fig. 9 displays *P* velocity maps at different depths and Fig. 10 is a section-line parallel to the seismicity cross-section in Fig. 6. We observe a relatively low-velocity zone located east of the Zendan fault system on the 0, 5 and 10 km depth slices. This low velocity is located at the edge of the seismicity and, therefore, is not very well resolved. But the most interesting and largest feature is the high-velocity zone present in the 15 and 20 km depth slices, with velocities larger than 7 km s^{-1}, located in the northeast of the seismic network and well resolved (for a spreading factor less than 5). The boundary between the low-velocity zone and the high-velocity zone trends NW–SE in both the 15 and 20 km deep slices, parallel to the tectonic structure. This boundary moves northwards with depth. In the cross-section (Fig. 10), the low-velocity anomaly clearly dips NE. It is clearer between 10 and 20 km, because of the velocity contrast at that depth. It suggests a depth offset of about 15 km that seems to match the seismicity.

We evaluated the reliability of the resulting 3-D velocity model with different methods (Paul *et al.* 2001). First, we estimated the spread function (Toomey & Foulger 1989) of the resolution matrix, which is a more reliable estimate than the diagonal of the resolution matrix, and we consider that the tomography is reliable where the spread function is smaller than 5. This gives an estimate of the confidence of the results but does not guarantee the resolution of the heterogeneity. To visualize this resolution, we calculated traveltimes for different synthetic velocity models using the same event-station couples as in the actual data set. We added random noise (0.2 s for *P* and 0.4 s for *S*) to synthetic traveltimes and inverted using SIMULPS12 with the same parameters as for the real data. We compare the results obtained for 2 different initial realistic synthetic models (one with reverse faulting, another one with a vertical offset) and confirm that we can discriminate between a thrust and an offset (Fig. 11). We are, therefore, confident that our cross-section indicates the north-eastward underthrusting of low-velocity material (the upper crust) beneath higher velocity material (the lower crust), and is associated with seismicity. However, our resolution does not allow determination of the dipping angle of the thrust.

DISCUSSION

Velocity structure

The crustal velocity structure obtained by the 1-D inversion includes a 10 km thick layer with a *P* wave velocity of 5.7 km s^{-1} overlying a 6.4 km s^{-1} basement. If the thickness of the sedimentary layer (∼10 km assumed from the 5.7 km s^{-1} velocity) is similar to that of the Central Zagros, its velocity is slightly higher than the 4.7 km s^{-1} observed in Qir (Hatzfeld *et al.* 2003). On the other hand, the lower layer of velocity 6.4 km s^{-1} is similar to the 6.5 km s^{-1} observed in

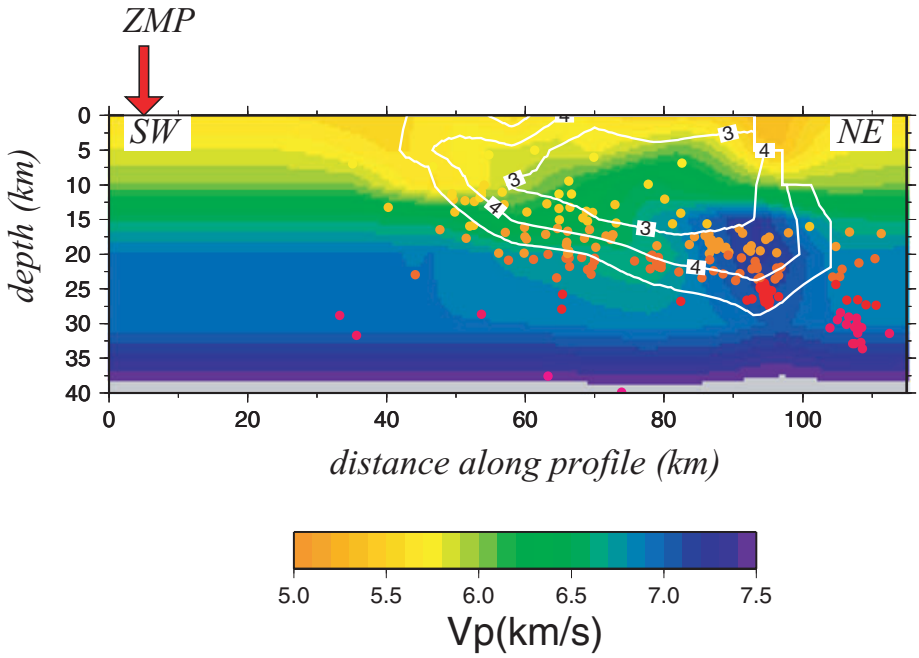

Figure 10. Cross-section of the 3-D velocity structure trending as Fig. 6. Results are reliable for a spread function less than 5 (white contour). The hypocenters are reported. There is a clear indication of a northward dipping anomaly related to the seismicity.

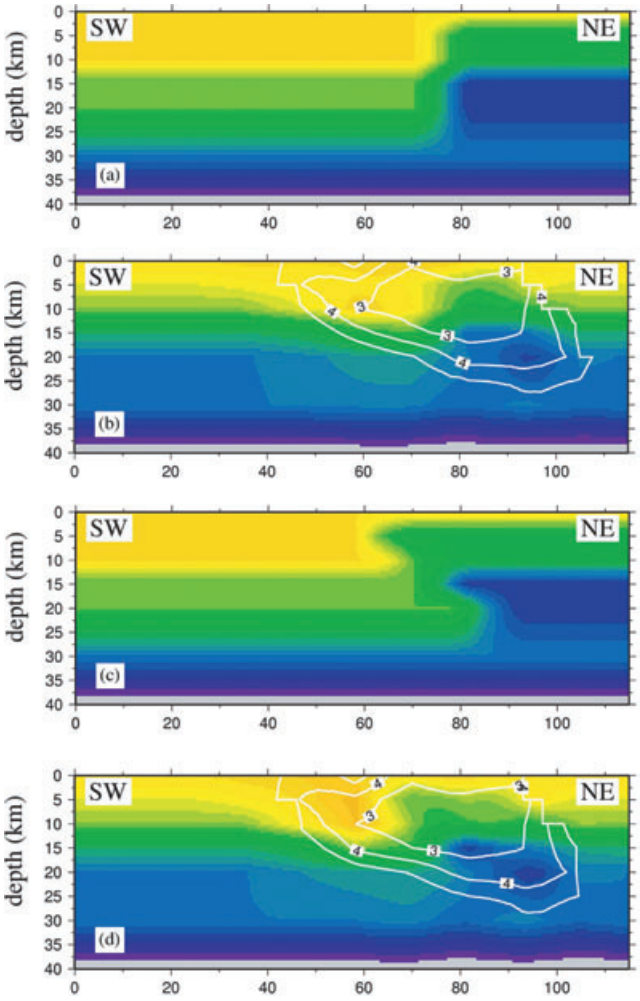

Figure 11. Synthetic tests of cross-sections. We show for both a step and a reverse thrust, the initial and the resulting models.

the Central Zagros. We have some information about the velocity structure of the shallow sediments of the Makran accretionary prism offshore (Kopp *et al.* 2000; Platt *et al.* 1988), but not for the oceanic crustal structure beneath, or inland; so we cannot compare our results directly with the Makran accretionary prism as a whole.

The 1-D inversion of local earthquake traveltimes provides the best available layered model for the area (Table 1). However, residuals clearly show a consistent pattern that suggests local heterogeneities. The 3-D inversion (Figs 9–11) suggests that the SW low-velocity body ($Vp < 6.5$ km s^{-1}), associated with the upper crust, underthrusts the NE high-velocity body ($Vp > 6.7$ km s^{-1}) associated with lower crust. The boundary between the two bodies strikes NW–SE, parallel to the shallow ZMP fault system, but it is located further north. It is also associated with dipping seismicity (Fig. 10). The southwestward projection of the inferred thrust plane, as well as of the associated seismicity, crosses the surface approximately in the area of the ZMP fault zone, suggesting a link between the two. The 3-D inversion reveals that this anomaly is not restricted to shallow depth and suggests that the ZMP has acted as a major reverse fault in the past as deduced from geological observations (Shearman 1977; Molinaro *et al.* 2004; Regard *et al.* 2004). The downdip length of the velocity contrast is approximately 10–15 km, comparable to the underthrusting imaged further north across the Main Zagros Reverse Fault by Paul *et al.* (2006).

Whereas relative velocities, or velocity contrasts, are reasonably well imaged with 3-D inversion techniques, absolute velocities, especially with depth, are not reliably constrained because of the low number of crossing paths in each block. The 7 km s^{-1} velocity observed at depth is slightly faster than is usually assumed for the lower crust. But this high velocity could be related to the ophiolites observed at the surface near the ZMP fault system. The low-velocity zone in the west of the network could be perturbated by the thick sedimentary layer in the Gulashkard basin (located between the ZMP and the JS fault systems) or unconsolidated material near the Zendan fault system (McCall 1985).

Seismicity

The microseismicity shows diffuse activity distributed within a large region from the Zagros to the Jaz-Murian basin. No clear single alignment can be inferred from the earthquake distribution and the pattern of focal mechanisms is complex. Therefore, we cannot use seismicity to infer clear individual strike-slip faults related to the surface expression of the ZMP and JS fault systems. There is no evidence for a transform fault between the Zagros collision and the Makran subduction, as might be expected for such a sudden continental-oceanic transition as is seen in other areas such as Greece (Baker *et al.* 1997) or New-Zealand (Anderson *et al.* 1993).

No microearthquake activity was recorded (during our recording period) beneath the Jaz-Murian basin, either at shallow or intermediate depth. This confirms the low teleseismic activity related to the Makran subduction (Byrne *et al.* 1992; Quittemeyer 1979). It suggests that the subduction is either locked (though this is not supported by the GPS measurements, Vernant *et al.* 2004; Bayer *et al.* 2006) or aseismic, probably because of the underplating of sediments (e.g. Kopp *et al.* 2000).

The ZMP fault zone is considered as a major tectonic and kinematic boundary between the Zagros and the Makran (Byrne *et al.* 1992; Vernant *et al.* 2004; Regard *et al.* 2004, 2005; Molinaro *et al.* 2004; Bayer *et al.* 2006). We recorded no microseismicity related to the ZMP fault system, reflecting the low teleseismically located activity over longer period of time (Engdahl *et al.* 1998). The only focal mechanism (#183) possibly associated with the ZMP is right-lateral strike-slip, consistent with the only CMT solution in this area and with the geologically inferred motion on the fault.

The depth of the microearthquakes undoubtedly increases from SW (∼10 km) to NE (∼40 km). This pattern is very different from what is observed in the Zagros Fold Belt where hypocenters are confined to the upper metamorphic crust (8–15 km) located beneath the thick layer of sediments (Tatar *et al.* 2004). This unusual pattern of increasing depth to the NE is consistent with teleseismic observations (Talebian & Jackson 2004) approximately 50 km north of our study area (Fig. 4). It suggests that seismicity is related to the underthrusting of the southwest Arabian crust under Central Iran. The prolongation to the surface of this thrust plane is located near the ZMP.

To determine the strain pattern, we separate the focal mechanisms into 2 different families (Figs 12a and b) depending on their type: (1) strike-slip mechanisms, with both *T*- and *P*-axes plunging less than 45°, and (2) reverse mechanisms, with the *P*-axis plunging less than 45° but the *T* axis plunging steeper. The majority of the shallow strike-slip mechanisms are located in the south and the majority of the deeper reverse mechanisms are in the north. Furthermore, these mechanisms are not uniformly spread over these areas, but are concentrated into a few clusters (which limits their interpretation).

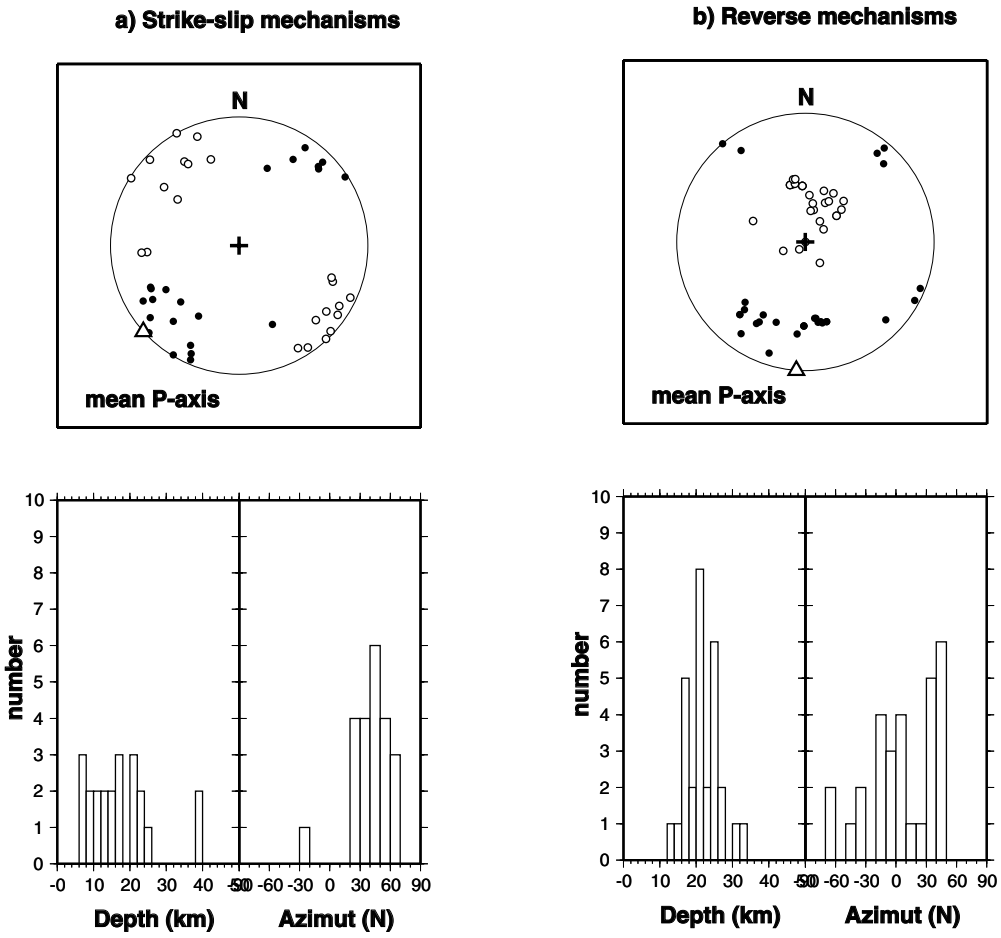

Figure 12. Main characteristics of the fault plane solutions for the strike-slip mechanisms and the reverse mechanisms. The reverse mechanisms are slightly deeper than the strike-slip mechanisms. The *P*-axes trend ∼NS whereas they trend ∼N45° for the strike-slip mechanisms. Black and white dots are *P*- and *T*-axis respectively.

The strike-slip mechanisms are generally located within the top 25 km of the crust whereas the reverse mechanisms are generally deeper, down to 35 km. We also computed a 'mean' direction of *P* axes for the strike-slip and for the reverse mechanisms (Fig. 12). The scatter is substantial, but we think that there is a significant difference in the orientations of the *P*-axes between the 2 families. The average orientation of *P*-axes of strike-slip mechanisms trends approximately 40°, whereas it trends 4° for the reverse mechanisms (Figs 12a and b).

Deformation pattern

Our focal mechanisms are related to small magnitude earthquakes and probably cannot be interpreted to show motion on single, major faults. If they reflect the mean *P*-axis orientation, they should be compared to the orientations of the principal compressive stress inferred from geological observations (Regard *et al.* 2004) or to the shortening direction deduced from GPS measurements (Bayer *et al.* 2006).

From the ZMP fault system, Regard *et al.* (2004) inferred that the present-day $\sigma 1$ trends N45°. It is associated with an oblique convergence on the ZMP and the Jiroft Sabzevaran fault systems. This oblique convergence is accommodated within a wide zone. From Miocene to Pliocene, the deformation was partitioned between the ZMP faults, which accommodated mostly strike-slip motion, and en echelon folding. Since the upper Pliocene, the regime has been more homogeneously transpressional. These results are consistent with GPS measurements that give also an orientation of the shortening of ∼N45°.

Fig. 13 shows, on a single stereographic projection, the mean orientations of the principal compressive stress obtained from the fault plane solutions (mean orientation of *P* axes), the tectonic-geological observations ($\sigma 1$) and the local GPS convergence motion between Arabia and Central Iran. The mean *P*-axis direction for the deeper reverse mechanisms is similar to the direction of the convergence deduced from GPS observations between Arabia and Central Iran, which is N10° (Vernant *et al.* 2004; Bayer *et al.* 2006), whereas the mean *P*-axis for the shallower strike-slip mechanisms is similar to the present-day local $\sigma 1$ direction inferred from tectonic observations, which is N45° (Regard *et al.* 2004). Therefore, we observe that the deeper reverse mechanisms appear directly related to the convergent motion between Arabia and Iran, so that strain (GPS motion) and stress (focal mechanisms *P*-axes) are coaxial. By contrast, the shallow mechanisms, which consistently agree with tectonic observations made at surface, differ from the overall convergent motion and, therefore, strain and stress differ in orientation.

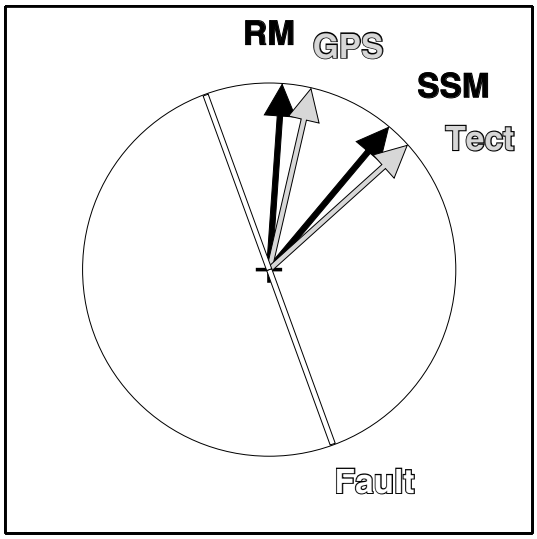

Figure 13. Vectors of the *P*-axes for the focal mechanisms (RM are deep reverse mechanisms and SSM are shallow strike-slip mechanisms) and of the GPS convergence between Arabia and Jaz Murian (Bayer *et al.* 2006) as well as the Quaternary stress pattern on the ZMP fault zone (Regard *et al.* 2004). There is a clear agreement between the shallow strike-slip focal mechanisms and the shallow tectonic observations on one hand, and between the deeper reverse focal mechanisms and the GPS convergence direction on the other hand. The oblique motion relative to the surface fault results in a slight partitioning at surface due to the weakness of the pre-existing ZMP fault system.

Partitioning

The agreement between the deeper mechanisms and the convergent motion, tells us that the motion of the lower crust is a reverse pure-shear consistent with the overall plate (or block) Arabia to Central Iran relative motion. But the difference at the surface between the shallow $\sigma 1$ orientation and the overall relative motion tells us that the upper crust does not accommodate the shortening in the same way, but that there is oblique convergence. The motion of Arabia relative to Central Iran is presently $\sim$N10°, and therefore oblique to the ZMP fault system, which trends N160°. The difference in azimuth between the ZMP fault orientation and the direction of motion (GPS) is therefore $\alpha = 20° + 10° = 30°$, which is the obliquity of the convergence. The angle between the faults and the principal stress $\sigma 1$ (both shallow mechanisms and tectonics) is $\theta = 20° + 45° = 65°$ (Fig. 13).

Oblique convergence in continental domains that is accommodated by anything except pure dip-slip motion on faults perpendicular to the overall convergence implies pre-existing faults or zones of weakness. The associated transpression could result in a complex pattern of both reverse and strike-slip faulting called a 'flower structure' (e.g. Woodcock & Fisher 1986). Analogue modelling suggests that these 'flower structures' occur when there is no decoupling at depth (Richard & Cobbold 1990). Oblique overall motion can also result in 'partitioning', or spatial separation, between pure strike-slip and pure shortening, with parallel strike-slip faults and reverse faults or folds accommodating strain in varying proportions (e.g. Fitch 1972; Teyssier & Tikoff 1998; Jackson 1992; Miller 1998). This partitioning may imply a ductile layer at depth (Richard & Cobbold 1990).

In our case, following Tikoff & Teyssier (1994) who computed analytical solutions using the deformation matrix approach, with $\alpha = 30°$ and $\theta = 65°$ (see above), we have about 30 per cent of strike-slip partitioning. This value is not high, which may explain why transpression on a single oblique–slip fault (Regard *et al.* 2004) is the main mechanism visible at surface. This ratio of 30 per cent is consistent with the component of slip perpendicular to the fault being about 50 per cent of the along-slip component of the motion as deduced form both the tectonic (Regard *et al.* 2004, 2005) and the GPS (Bayer *et al.* 2006) observations.

Finally, only a superficial examination of the transition between the continental collision of the Zagros and the subduction of Makran suggests the existence of a major strike-slip fault to accommodate the differential motion between the two. This is apparently supported by the large ophiolite bodies that are located along the MZRT in Zagros and in Oman. But these ophiolite bodies lie north of the Persian Gulf in the Zagros and south of the Gulf of Oman in the Makran and look offset in space. Actually, these ophiolites were emplaced at the same time, probably with the same mechanism, and the closure of the Persian Gulf region and the differential sedimentation that followed this closure hide some of the main characteristics of the transition.

CONCLUSION

Our seismological study shows that the differential motion between the Zagros continental collision and the Makran subduction the ZMP fault system is not accommodated by a major lithospheric-scale transform fault. On the contrary, the NE deepening seismicity, down to an unusually large depth of 40 km within the crust, is associated with a strong velocity anomaly, which could be connected at the surface to the ZMP fault system, suggesting an overall different geometry. They suggest a diffuse, rather than localized, transition, at depth, between the suture located to the west (the Main Zagros Reverse Fault located north of Zagros) and the Makran active subduction to the east.

Because the Main Zagros Reverse Fault is the surface trace of the former subduction of Arabia beneath Iran before the collision, this diffuse transition observed in the crust probably indicates a diffuse transition at a lithospheric scale as well. This result is also consistent with the tectonic observations regarding the evolution in time of the ZMP fault system, and of the width of the transpression zone, which acted first (during Miocene) as a pure reverse fault and later (since upper Pliocene) as a transpressive fault (Regard *et al.* 2004). Because the onset of the continental collision is recent (Miocene), there is no large finite differential motion across the ZMP fault zone which probably reflects mostly the surface shape of the pre-collision boundary, located along what was previously the main reverse fault.

The difference in the accommodation of the shortening between the lower crust and the upper crust also suggests different mechanical properties. The difference between strain and stress orientations at surface suggests that the shallow rigid crust is cut by mechanical weakness probably resulting from pre-existing inherited faults that perturb the stress field. The co-linearity between motion and stress at depth shows that the lower crust accommodates the shortening in a much simpler (and, therefore, probably continuous in time) way.

ACKNOWLEDGMENTS

This study was supported by IIEES (International Institute of Earthquake Engineering and Seismology, Iran), the program Dyeti (INSU-CNRS, France) and the French Embassy in Tehran in the frame of a cooperative research programme. The paper benefited from stimulating discussions with C. Authemayou, O. Bellier,

J. Jackson, P. Molnar and V. Regard. Careful reviews by M. Molinaro and R. Walker helped to improve the manuscript. We thank M. Ghafory Ashtiany president of IIEES for his help. We would like to thank K. Assatourian, B. Bettig, J.-M. Douchain, M. Ghasemi, H. Heidary-Moghadar, A. Kaviani, M. Masoudi, M. Parvazeh M. Taghaboni, M. Vallée, C. Voisin and M. Zolfaghari, for their help in the field work. This work would not have been possible without the help of the Hormozgan province and especially of the governor of Minab.

REFERENCES

Ambraseys, N.N. & Melville, C.P., 1982. *A history of Persian Earthquakes*, Cambridge Earth Science Series, Cambridge University Press, London.

Anderson, H., Webb, T. & Jackson, 1993. Focal mechanisms of large earthquakes in the South Island of New Zealand: implications for accommodation of Pacific-Australia plate motion, *Geophys. J. Int.,* **115**(1), 1032–1054.

Baker, C., Hatzfeld, D., Lyon-Caen, H., Papadimitriou, E. & Rigo, A., 1997. Earthquake mechanisms of the Adriatic sea and western Greece: implications for the oceanic subduction-continental collision transition, *Geophys. J. Int.,* **131,** 559–594.

Bayer, R. *et al.*, 2006. Active deformation in Zagros-Makran transition zone inferred from GPS measurements, *Geophys. J. Int.,* **165,** 373–381.

Berberian, M., 1995. Master blind thrust faults hidden under the Zagros folds: active basement tectonics and surface morphotectonics, *Tectonophysics,* **241,** 193–224.

Berberian, M. & Tchalenko, J.S., 1976. Earthquakes of the Bandar-Abbas-Hajiabad region (Zagros-Iran), *Geol. Surv. of Iran, Report No.,* **39,** 372–396.

Berberian, M., Papastamatiou, D. & Qoraishi, M., 1977, Khurgu (North Bandar Abbas-Iran) earthquake of March 21, 1977: a preliminary field report and a seismotectonic discussion, *Geol. Surv. of Iran, Report No.,* **40,** 7–50.

Blanc, E.J.-P., Allen, M.B., Inger, S. & Hassani, H., 2003. Structural styles in the Zagros Simple Folded Zone, *Iran, J. Geol. Soc. London,* **160,** 401–412.

Byrne, D.E., Sykes, L.R. & Davis, D.M., 1992. Great Thrust Earthquakes and Aseismic Slip Along the Plate Boundary of the Makran Subduction Zone, *J. geophys. Res.,* **97**(B1), 449–478.

Engdahl, E.R., Van Der Hilst, R. & Buland, R., 1998. Global teleseismic earthquake relocation with improved travel times and procedures for depth determination, *Bull. seism. Soc. Am.,* **88,** 722–743.

Evans, J.R., Eberhart-Phillips, D. & Thurber, C.H., 1994. User's manual for SIMULPS12 for imaging Vp and Vp/Vs: A derivative of the 'Thurber' Tomographic inversion SIMUL3 for local earthquakes and explosions, USGS, Open-file Report, 94–431.

Farhoudi, G. & Karig, D.E., 1977. Makran of Iran as an active arc system, *Geology,* **5,** 664–668.

Falcon, N.L., 1974. An outline of the Geology of the Iranian Makran, *Geogr. J.,* **140,** 284–291.

Fitch, T., 1972, Plate Convergence, Transcurrent Faults, and the internal Deformation Adjacent to Southeast Asia and the Western Pacific. *J. geophys. Res.,* **77,** 4432–4460.

Gansser, A., 1964. *The geology of the Himalayas*, Intersciences, New York, p. 289.

Harms, J.C., Cappel, H.N. & Francis, D.C., 1984. The Makran coast of Pakistan: its stratigraphy and hydrocarbon potential, in *Marine Geology and Oceanography of Arabian sea and Coastal Pakistan*, pp. 3–26, eds Haq, B.U. & Milliman, J.D., Van Nostrand Reinhold, New York.

Hatzfeld, D., Tatar, M., Priestley, K. & Ghafory Ashtiany, M., 2003. Seismological constraints on the crustal structure beneath the Zagros Mountain belt (Iran), *Geophys. J. Int.,* **155,** 1–8.

Hessami, K., Nilforoushan, F. & Talbot, C., 2006. Active deformation within the Zagros Mountains deduced from GPS measurements, *J. geol. Soc. Lond.,* **163,** 143–148.

Jackson, J.A., 1980. Reactivation of basement faults and crustal shortening in orogenic belts, *Nature,* **283,** 343–346.

Jackson, J., 1992. Partionning of strike-slip and convergent motion between Eurasia and Arabia in Eastern Turkey and the Caucasus, *J. geophys. Res.,* **97,** 471–479.

Jacob, K.H. & Quittemeyer, R.L., 1979. The Makran region of Pakistan and Iran: trench-arc system with active plate subduction, in *Geodynamics of Pakistan*, eds Farah, A. & de Jong, K.A., Geological Survey of Pakistan, Quetta.

Kadinsky-Cade, K. & Barazangi, M., 1982. Seismotectonics of Southern Iran, *Tectonics,* **5,** 389–412.

Kao, H., Jack Shen, S.S. & Ma, K.-F., 1998. Transition form oblique subduction to collision: Earthquakes in the southernmost Ryuku arc-Taiwan region, *J. geophys. Res.,* **103,** 7211–7229.

Kissling, E., 1988. Geotomography with local earthquake data, *Rev. Geophys.,* **26,** 659–698.

Kopp, C., Fruehn, J., Flueh, E.R., Reichert, C., Kukowski, N., Bialas, J. & Klaeschen, D., 2000. Structure of the Makran subduction zone from wide-angle and reflection seismic data, *Tectonophysics,* **329,** 171–191.

Lee, W.H.K. & Stewart, S.W., 1975. HYPO71 (Revised): a computer program for determining hypocenter, magnitude and first motion pattern of local earthquakes, US Geological Survey, Open File Report, 75–311.

Maggi, A., Jackson, J.A., Priestley, K. & Baker, C., 2000, A re-assessement of focal depth distributions in Southern Iran, the Tien Shan and Northern India, Do earthquakes really occur in the continental mantle?, *Geophys. J. Int.,* **143,** 629–661.

McCall, G.J.H., 1985. Explanatory text of the Minab quadrangle map 1:250,000, *Geol. Surv. of Iran*, Geological Quadrangle, No. J 13.

McCall, G.J.H. & Kidd, R.G.W., 1982. The Makran southeastern Iran: the anatomy of a convergent plate margin from Cretaceous to Present, in *Trench Forearc Gelogy*, pp. 387–397. ed. Legget, J.K., Geol. Soc of London, Spec. Publ.

McQuarrie, N., 2004. Crustal scale geometry of the Zagros fold-thrust belt, Iran, *J. Struct. Geol.,* **26,** 519–535.

Miller, D.D., 1998. Distributed shear, rotation, and partitioned starin along the San Andreas fault, California, *Geology,* **26,** 867–870.

Molinaro, M., Guezou, J.C., Leturmy, P., Eshraghi, S.A. & Frizon de Lamotte, D., 2004. The origin of changes in structural style across the Bandar Abbas syntaxis, SE Zagros (Iran), *Marine and Petroleum Geology,* **21,** 735–752.

Molinaro, M., Leturmy, P., Guezou, J.-C. & Frizon de Lamotte, 2005. The structure and kinematics of the south-eastern Zagros fold-thrust belt, Iran: from thin-skinned to thick-skinned tectonics, *Tectonics,* **24,** NIL42–NIL60.

Niazi, M., 1980. Microearthquakes and crustal structure off the Makran coast of Iran, *Geophys. Res. Lett.,* **7,** 297–300.

Paul, A., Cattaneo, M., Thouvenot, F., Spallarossa, D., Béthoux, N. & Fréchet, J., 2001. A three-dimensional velocity model of the southwestern Alps from local earthquake tomography, *J. geophys. Res.,* **106**(B9), 19 367–19 389.

Paul, A., Kaviani, A., Hatzfeld, D., Vergne, J. & Mokhtari, M., 2006. Seismological evidence for crustal-scale thrusting in the Zagros mountain belt (Iran), *Geophys. J. Int.,* **166,** 227–237.

Platt, J.P., Leggett, J.K. & Alam, S., 1988. Slip vectors and fault mechanics in the Makran accretionary wedge, southwest Pakistan, *J. geophys. Res.,* **93,** 7955–7973.

Quittemeyer, R.C., 1979. Seismicity variations in the Makran region of Pakistan and relation to great earthquakes, *Pure appl. Geophys.,* **117,** 1212–1228.

Quittemeyer, R.C. & Jacob, K.H., 1979. Historical and modern seismicity of Pakistan, Afghanistan, northwestern India, and southern Iran, *Bull. seism. Soc. Am.,* **69,** 773–823.

Regard, V., Bellier, O., Thomas, J.-C., Abbassi, M.R., Mercier, J., Shabanian, E., Feghhi, Kh. & Soleymani, Sh., 2004. The accommodation of Arabia-Asia convergence in the Zagros-Makran transfer zone, SE Iran: a transition between collision and subduction through a young deforming system. *Tectonics,* **23,** TC4007, (24p.) doi :10.1029/2003TC001599.

Regard, V. *et al.*, 2005. Cumulative right-lateral fault slip rate across the Zagros – Makran transfer zone and role of the Minab-Zendan fault system

within the convergence accommodation between Arabia and Eurasia (SE Iran). *Geophys. J. Int.,* **160,** 1–25.
Richard, P. & Cobbold, P., 1990. Experimental insights into partitioning of fault motions in continental convergent wrench zones, *Ann. Tectonicae, 1990,* **4,** 35–44.
Sattarzadeh, Y., Cosgrove, J.W. & Vita-Finzi, C., 2000. The interplay of faulting and folding during the evolution of the Zagros deformation belt, in '*Forced folds and fractures*', Vol. 169, pp. 187–196, eds Cosgrove, J.W. & Ameen M. S., Geol. Soc. Spec. Pub.
Shearman, D.J., 1977. The geological evolution of Southern Iran, the report of the Iranian Makran expedition, *Geogr. J.,* **142,** 393–410.
Snyder, D.B. & Barazangi, M., 1986. Deep crustal structure and flexure of the Arabian plate beneath the Zagros collisional mountain belt as inferred from gravity observations, *Tectonics,* **5,** 361–373.
Stöcklin, J., 1968. Structural history and tectonics of Iran, a review, *Am. Assoc. Pet. Geol. Bull.,* **52,** 1229–1258.
Stöcklin, J., 1974. Possible ancient continental margin in Iran, in *Geology of Continental Margins*, pp. 873–877. eds Burke, C. & Drake, C., Springer-Verlag, New York.
Stoneley, R., 1981. The geology of the Kuh-e Dalneshin area of southern Iran, and its bearing on the evolution of southern Tethys, *J. geol. Soc. Lond.,* **138,** 509–526.
Talebian, M. & Jackson, J., 2004. A reappraisal of earthquake focal mechanisms and active shortening in the Zagros mountains of Iran, *Geophys. J. Int.,* **156,** 506–526.
Tatar, M., Hatzfeld, D., Martinod, J., Walpersdorf, A., Ghafori-Ashtiany, M. & Chéry, J., 2002. The present-day deformation of the central Zagros (Iran) from GPS measurements, *Geoph. Res. Lett.,* **29**(19),1927–1930.
Tatar, M., Hatzfeld, D. & Ghafory-Ashtiany, M.. 2004. Tectonics of the Central Zagros (Iran) deduced from microearthquake seismicity, *Geophys. J. Int.,* **156,** 255–266.
Teyssier, C. & Tikoff, B., 1998. Strike-slip partitioned transpression of the San Andreas fault system: a lithospheric approach, in *Continental transpressional tectonics*, Vol. 135, pp. 143–158, eds Holdsworth, R.E., Strachan, R.A. & Dewey, J.F., Geol. Soc. London, Spec. Pub.
Thurber, C.H., 1993. Local earthquake tomography: Velocities and Vp/Vs – Theory, in *Seismic Tomography: Theory and Practice,* pp. 563–583, eds, Iyer, H.M. & Irahara, K., Chapman & Hall, New York.
Tikoff, B. & Teyssier, C., 1994. Strain modeling of displacement-field partitioning in transpressional orogens, *J. Struc. Geol.,* **16,** 1575–1588.
Toomey, D.R. & Foulger, G.R., 1989. Tomographic inversion of local earthquakes data from the Henill-Grensdalur central volcano complex, Iceland, *J. geophys. Res.,* **94,** 17 497–17 510.
Vernant, P. *et al.*, 2004. Present day crustal deformation and plate kinematics in the middle east constrained by GPS measurements in Iran and Northern Oman, *Geophys, J. Int.,* **157,** 381–398.
Waldhauser, F. & Ellsworth, W.L., 2000. A double difference earthquake location algorithm: Method and application to the northern Hayward fault, California, *Bull. seism. Soc. of Am.,* **90,** 1353–1368.
Walker, R. & Jackson, J., 2002. Offset and evolution of the Gowk fault, S.E. Iran: a major intra-continental strike-slip system. *Journal of Structural Geology,* **24,** 1677–1698.
Walpersdorf, A. *et al.*, 2006. Difference in the GPS deformation pattern of North and Central Zagros (Iran), *Geophys. J. Int.*, submitted.
White, R.S., 1982. Deformation of the Makran accretionary sediment prism in the Gulf of Oman, in Leggett, J.K., ed., Trench-Forearc Geology: Sedimentation and Tectonics on Modern and Ancient Active Plate Margins, *Geol. Soc. Spec. Publ. London,* **10,** 357–372.
White, R.S. & Ross, D.A., 1979. Tectonics of the Western Gulf of Oman, *J. geophys. Res.,* **84,** 3479–3489.
Woodcock, N. & Fisher, M., 1986. Strike-slip duplexes, *J. Struct. Geol.,* **8,** 725–735.
Yamini-Fard F., 2003. Sismotectonique et structure lithosphérique de deux zone de transition dans le Zagros (Iran): la zone de Minab et la zone de Qatar-Kazerun, *PhD Thesis,* Joseph Fourier University, Grenoble I.
Yamini-Fard, F., Hatzfeld, D., Tatar, M. & Mokhtari, M., 2006. Microseismicity at the intersection between the Kazerun fault and the Main Recent Fault (Zagros-Iran), *Geophys. J. Int.,* **166,** 186–196.

SUPPLEMENTARY MATERIAL

The following supplementary material is available for this article:

Appendix S1. Lower hemisphere of focal spheres. Solid and open circles are reliable compressional and dilatational first motions; + and − are uncertain. Solid and open triangles are *P*- and *T*-axes, respectively.

This material is available as part of the online article from: http://www.blackwell-synergy.com/doi/abs/10.1111/j.1365-246X.2006.03232.x
(this link will take you to the article abstract).

Please note: Blackwell Publishing are not responsible for the content or functionality of any supplementary materials supplied by the author. Any queries (other than missing material) should be directed to the corresponding author for the article.